J. Fluid Mech. (1983), *vol.* 134, *pp.* 1–31
Printed in Great Britain

Noise generation by a low-Mach-number jet

By JOHN LAUFER AND TA-CHUN YEN†
Department of Aerospace Engineering, University of Southern California, Los Angeles, CA 90089-1454

(Received 22 November 1982)

Using a 'clean' jet facility the relationship between the jet flow and its radiation field was studied experimentally in the Mach-number range $0.05 < M_j < 0.20$ and a Reynolds-number range $6 \times 10^4 < Re_D < 2.3 \times 10^5$. The various acoustic source parameters such as strength, frequency and Mach number were varied systematically, and the far-field pressure measured simultaneously. On the basis of these measurements the nature of the sources in the initial shear layer could be characterized. The principal results, equally valid for unexcited and excited jets, are as follows: the acoustic sources are not convected but are located within a confined volume fixed with respect to the nozzle even though they are being generated by moving disturbances in the jet; they are associated with the nonlinear saturation of the unstable wave amplitudes of the shear layer occurring at the vortex-pairing locations; the radiation intensity varies nonlinearly with the source strength and is highly directional, exponential in character.

1. Introduction

Since Lighthill's (1952) mathematical formulation of the aeroacoustic problem, considerable effort has been spent to arrive at a feasible physical interpretation of his formal result and, in particular, of his quadrupole source term. Such an understanding is essential if one is to make any further progress in the noise reduction of jets.

In fact, any experiment addressing this question faces a very difficult problem: what measurements should be made in order to clarify the nature of the quadrupole sources? The difficulty is the following: measurements in the far field, no matter how detailed and sophisticated, cannot lead to a unique picture concerning the nature of the acoustic sources. One is forced therefore to make measurements at the source location as well. This, however, proves to be a most elusive task. Since the noise production is associated with a volume integral, point measurements (or even two- or three-point correlation measurements) are insufficient to lead one to the desired picture of the sources.

A major step toward a better understanding of the problem was made by Crow & Champagne (1971). They have suggested that the jet acts as an amplifier for any disturbance it is subjected to, especially if the disturbance has a certain preferred frequency. In particular, they found that the perturbed amplitudes grow rapidly with distance from the nozzle; subsequently they saturate and then decay. On the basis of these experimental findings Crow (1972) suggested the so-called 'line-antenna' model to describe the acoustic behaviour of a jet. In its simplest form, it consists of a travelling wave that increases and decreases in amplitude in a Gaussian manner

† Present address: Beijing University, Beijing, People's Republic of China.

in the direction of convection. Crow made some estimates of the increased noise radiation due to such an amplifier with promising results. Unfortunately, no further work was done in this direction for some years until Crighton described it in some detail in his 1975 review paper, and later Ffowcs Williams & Kempton (1978) modified it and extended it to include a small random phase fluctuation. More will be said about this work later.

A few years after the Crow & Champagne paper appeared, Brown & Roshko (1974) as well as Winant & Browand (1974) showed in a convincing manner the presence in a mixing layer of large, coherent structures that interact with each other and are mainly responsible for the shear-layer growth. Subsequently, the same type of interaction was observed in a circular jet by Browand & Laufer (1975). (Actually, the vortex ring-like structures were known much earlier by a number of investigators but their significance was not appreciated at that time.) In particular, they have noted large acceleration–deceleration sequences during the pairing process. On the basis of these observations, Laufer (1974) suggested that the interaction process might be closely associated with the noise generation in the jet. Unfortunately, he could not give any direct evidence to substantiate his proposal at that time. Ffowcs Williams & Kempton in the (1978) paper mentioned earlier proposed a mathematical model for the vortex pairing and obtained some encouraging results in terms of the radiation intensity. However, as far as the directional intensity distribution is concerned, the antenna and the vortex-pairing model give significantly different results. It is therefore of great interest to investigate experimentally the reason behind this difference and to ascertain whether the difficulty lies in the physical interpretation of the acoustic source or its mathematical modelling.

Since the work of Crow & Champagne, a large number of experimental papers have appeared in the literature, examining the behaviour of jets under artificial excitation. One of the most interesting is that of Bechert & Pfizenmaier (1975), who have shown that, with a relatively small level of pure tone excitation, broadband jet noise can be amplified. The practical implication of this result is obvious. However, no supporting experiments were done to provide a physical explanation of this interesting result.

One of the most comprehensive and informative investigations of the flow field in the jet and of the radiation field, with and without excitation, was carried out by Moore (1977). He has convincingly shown that 'large-scale jet structures play an important part in the generation of jet noise'. However, his conclusion that 'there is no significant radiation from the instability wave over the Mach-number range 0.1–0.9 and the Strouhal-number range 0.1–3.5' is too hastily drawn, and is in direct contrast with the present results, at least in the lower Mach-number range. Further discussion on this point will be given in §3.

The feasibility of a definitive experiment was recognized by Laufer & Monkewitz (1980), who have analysed the measurements of Kibens (1980). Introducing an appropriate disturbance into the initial shear layer in a certain Reynolds-number range, Kibens was able to localize the pairing position of the ring vortices. At the same time, he measured strong spectral peaks in the far field corresponding to the pairing frequencies. The results suggested the possibility of studying the causality relationship between vortex pairing as an acoustic source and its far-field characteristics.

The present paper describes experiments designed to accomplish this. Taking special precautions to minimize upstream flow disturbances, the acoustic field of a

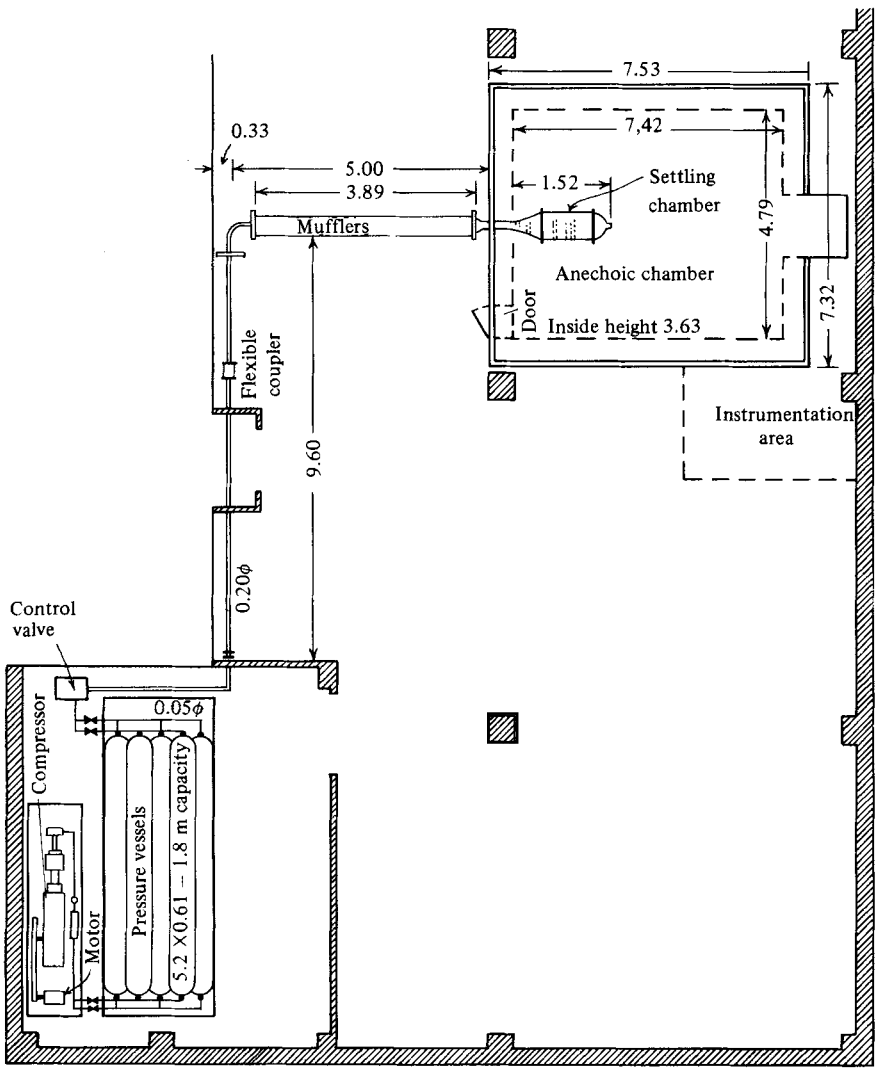

FIGURE 1. Jet facility.

jet in a Mach-number range as low as 0.05–0.2, corresponding to a diameter Reynolds number of 60000–230000, was investigated. In this flow range most of the radiation occurs along the first diameter of the jet, where the flow is found to be well organized. This fact enables one to draw some definitive conclusions concerning the character of the acoustic sources.

2. Facility and instrumentation

2.1. *Facility*

The jet facility is a blowdown system comprising a compressor, five pressure vessels, and a specially designed low-noise valve (figure 1). Extra effort has been made in order

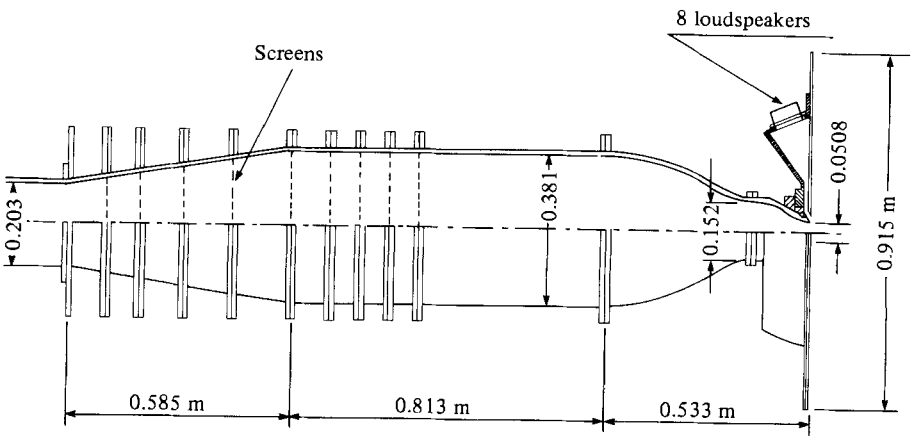

FIGURE 2. Settling chamber and nozzle assembly.

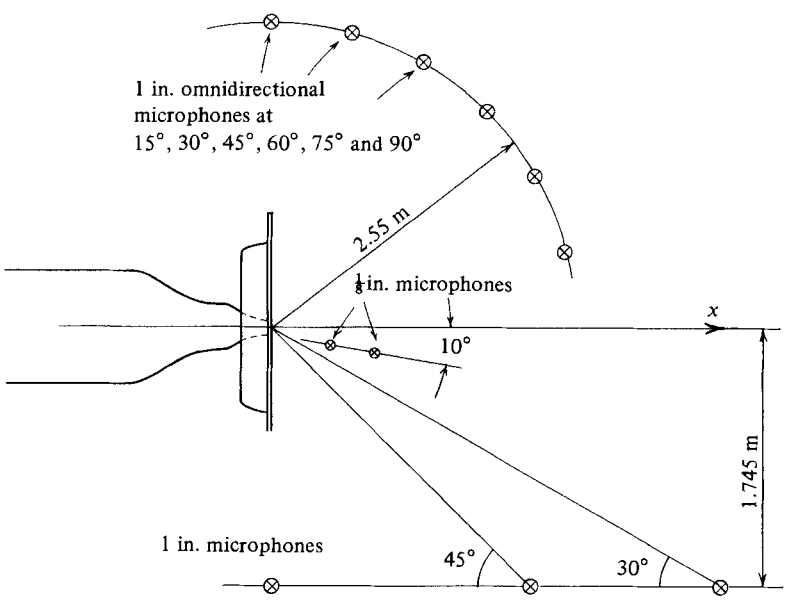

FIGURE 3. Geometry of the test set-up.

to minimize the upstream noise level and vorticity fluctuations in the duct system. The jet settling chamber has a diameter 0.38 m; at the end of the first contraction it becomes 0.152 m. The second contraction is interchangeable and has a 0.0508 m exit diameter in this experiment. The total contraction ratio is 56.25 (figure 2).

The flow field at the exit of the nozzle is uniform, with a turbulence intensity lower than 0.1 %. The exit boundary layer is laminar; the initial shear-layer momentum thickness is 0.15 mm at a jet velocity of 30 m/s, giving the relation $\theta_0/D = 0.98/Re_D^{\frac{1}{2}}$ The Reynolds number based on jet diameter ranges from 0.6×10^5 to 2.3×10^5. The jet velocities in most of the experiments were 18, 30, 50 and 70 m/s.

An axially symmetric acoustic chamber was fitted to the exit of the nozzle as shown in figure 2. Four low-frequency and four high-frequency loudspeakers, arranged

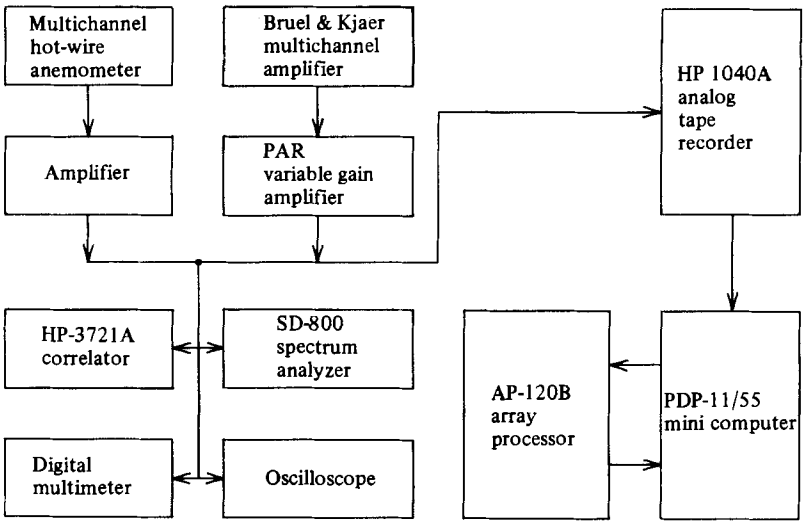

FIGURE 4. Data acquisition and processing.

azimuthally, generate a nearly uniform acoustic disturbance propagating in a direction at 70° to the jet axis through a 1 mm wide circular slot. Both the intensity and frequency of the disturbance were varied as described subsequently.

2.2. *Instrumentation*

All of the velocity measurements were made using a hot-wire anemometer with a two-directional traverse to control the axial and radial positions. The diameter of the hot wire was 2.5 μm. Near-field pressure fluctuations were measured by a $\frac{1}{8}$ in. B & K microphone. In the far field, a number of 1 in. B & K microphones were used. The positions of the microphones are shown in figure 3.

The hot-wire and microphone signals were recorded on a HP1040A analog tape recorder with a 20 kHz cutoff frequency, then fed into the PDP 11/55 minicomputer. Most of the data were digitized at a 60 kHz rate, which provided a 60 Hz resolution in the frequency domain. An Ap120B array processor made by Floating Point Company was used in the power and cross-spectra calculations, with a high pass-through rate. A block diagram showing the data acquisition and processing set-up is given in figure 4.

2.3. *Calibration*

Before analysing the near-field and far-field results, it is important to establish a reference for the forcing amplitude in order to estimate the effect of the acoustic excitation on the flow field and the noise radiation.

The horn speakers and the low-frequency loudspeakers were used for the high- or low-speed ranges respectively, and the forcing voltages recorded. The radiation efficiencies of the two sets of loudspeakers were quite different and varied with frequency. This was determined by measuring the acoustic pressure with flow by a 1 in. B & K microphone at a 30° angle from the jet axis and a 2.55 m radius from the source. The forcing voltage V_f is plotted versus the measured acoustic r.m.s. pressure in figure 5.

In order to monitor the effect of the acoustic excitation on the flow field, the saturation amplitude of the various eigenmodes $(\overline{u^2_{mn}})^{\frac{1}{2}}/U_j$ was chosen as a reference.

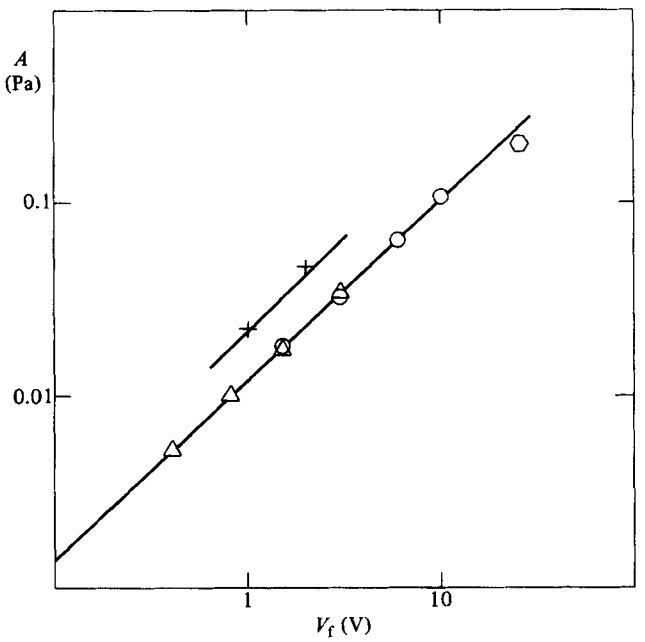

FIGURE 5. Intensity calibration of the low-frequency speakers; $\theta = 30°$, $R = 2.55$ m: +, $U_j = 18$ m/s; △, 30 m/s; ○, 50 m/s; ⬡, 70 m/s.

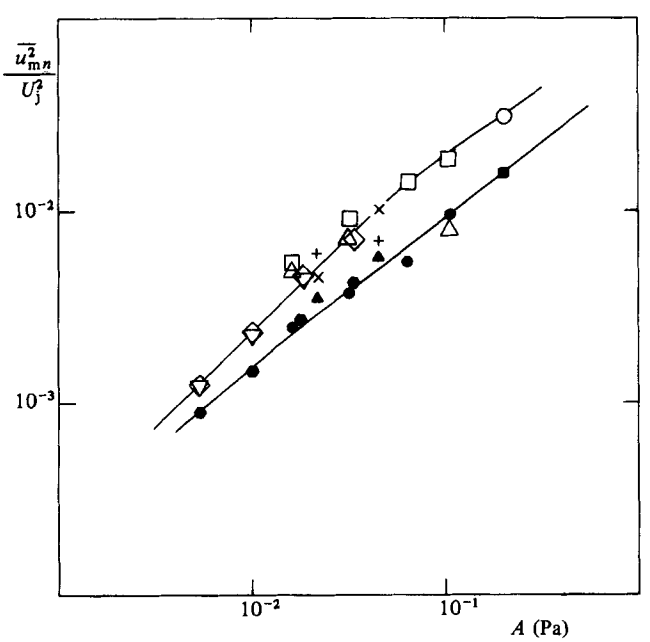

FIGURE 6. Relationship between forcing amplitude and eigenmode saturation for the following values of U_j:

f_0	f_1	f_2
■ 70 m/s	⬡ 70 m/s	○ 70 m/s
● 50 m/s	△ 50 m/s	□ 50 m/s
⬢ 30 m/s	◇ 30 m/s	▽ 30 m/s
▲ 18 m/s	+ 18 m/s	× 18 m/s

Here the subscript $n = 0, 1, 2$ denotes the fundamental, first and second subharmonic eigenmode. For a fixed jet velocity and forcing amplitude A, a moving hot wire was used to locate the (x, y)-position where the fundamental, first and second subharmonic eigenmodes attain their maximum amplitudes. Figure 6 shows the resulting calibration curve. It is of interest to note that, for a given A, the percentage of perturbations generated in the shear layer is independent of the jet velocity. In general, the excitation amplitudes used in the experiments produced a 20 %–500 % increase in the eigenmode amplitudes.

3. Measurements and results

It would seem that, in order to establish a causal relationship between the jet flow as an acoustic source and its far field, it is necessary to understand the *complete time-dependent flow field* of the jet in some detail. With the present meagre knowledge of turbulent shear flows, this would be a formidable task indeed.

The intention of the present experiments is to render the flow as organized as possible in the flow region that radiates measurable energy. That is to say, one is trying to establish a shear flow in which the saturation amplitude of each unstable wave occurs at the same location from cycle to cycle, a flow with minimum phase fluctuations. Kibens (1980) has shown that this is possible, if one excites the initial shear layer at its most-unstable frequency f_0, or at its first subharmonic. At the same time, the lower subharmonics get organized as well, but the phase fluctuations increase with distance downstream where the lower subharmonics develop. Now, in most practical jets, the preferred frequency f_p (the frequency at which maximum radiation is observed and which corresponds to the passage frequency of the large-scale structures near the end of the potential core), is at least near the fourth or even lower subharmonic of f_0, and the Kibens technique will not sufficiently minimize the phase fluctuations in the preferred mode. In the experiment, therefore, one will have to be satisfied with studying the radiation corresponding to the first and second subharmonic instability waves.

On the basis of this discussion it follows that, for an optimally designed experiment, the following conditions should be satisfied:

(i) the upstream turbulence level has to be as low as possible in order to minimize the phase fluctuations in the unexcited jet;

(ii) the ratio f_0/f_p must be kept small, which can be done by keeping the Reynolds number low;

(iii) the jet Mach number must be large enough that the radiation intensity is sufficiently high for reliable measurements.

It should also be mentioned that, since the initial shear layer is a highly tuned system, care has to be taken that the excitation frequency be as close to f_0 as possible in order to be able to lock into it. The success of the technique can easily be ascertained by comparing velocity or pressure spectra made in or near the jet: there should be a broadband attenuation below f_0 (except for the subharmonics, of course), as indeed the results show in §3.1. It is to be noted here, that in the Bechert & Pfizenmaier (1975) and Moore (1977) experiments the jet was excited near its preferred frequency with just the opposite result: presumably owing to amplitude and phase modulations between the various natural and the imposed perturbations, a broadband amplification occurs in the far-field spectra.

The disadvantage of the presently adopted technique is that one is restricted to relatively low Mach- and Reynolds-number ranges and is obliged to study the radiation mechanism within the first diameter of the jet and not in the region near

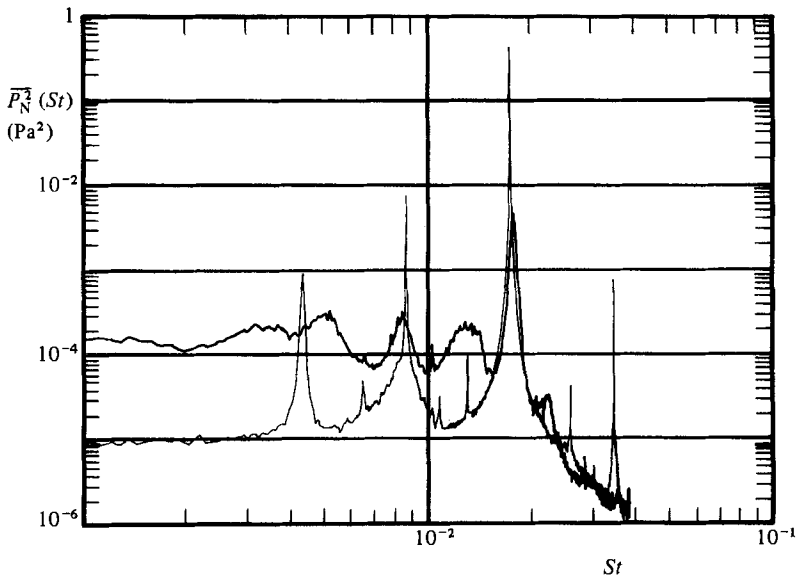

FIGURE 7. Near-field pressure spectra, $U_j = 70$ m/s, $x/D = 0.1$: ——, natural; ——, excited ($\overline{u_{m0}^2}/U_j^2 = 1.6 \times 10^{-2}$).

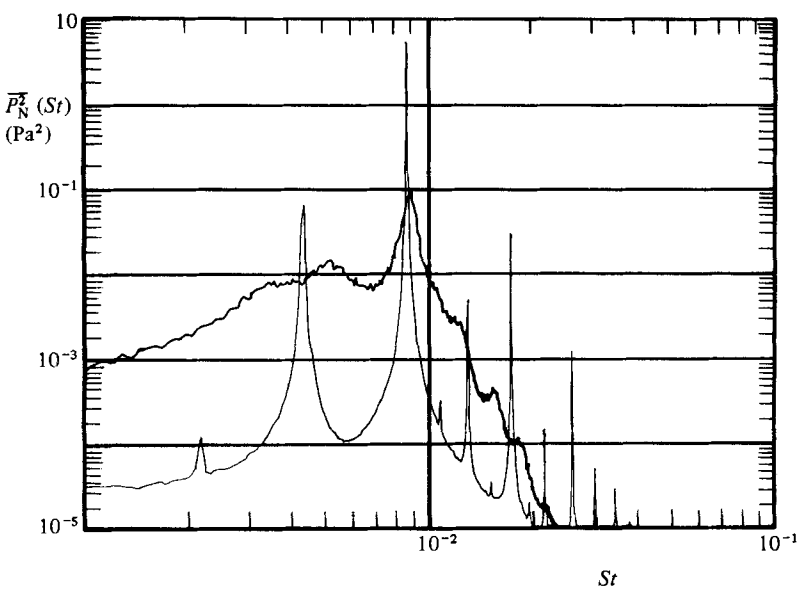

FIGURE 8. Near-field pressure spectra, $U_j = 70$ m/s, $x/D = 0.20$: ——, natural; ——, excited.

the end of the potential core where most of the noise is generated in conventional, higher-Mach-number jets. On the other hand, the method enables one to control the fluctuation amplitudes (or source strength) of the flow without changing the nature of the flow dynamics and to relate the unsteady flow directly to its acoustic field.

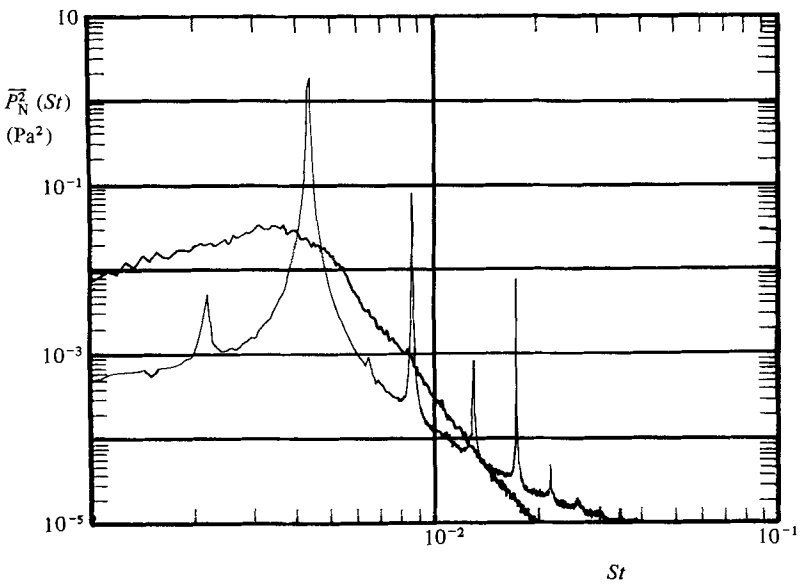

FIGURE 9. Near-field pressure spectra, $U_j = 70$ m/s, $x/D = 0.40$: ——, natural; ——, excited.

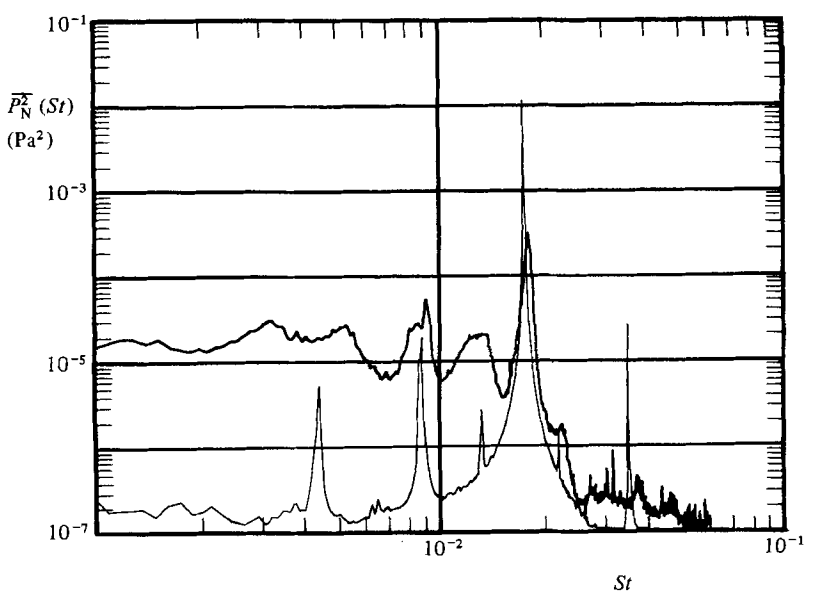

FIGURE 10. Near-field pressure spectra, $U_j = 50$ m/s; $x/D = 0.10$: ——, natural; ——, excited, $\overline{u_{m0}^2}/U_j^2 = 0.95 \times 10^{-2}$.

3.1. *The source region*

The initial shear layer is laminar in the range of the experiment and is inviscidly unstable. The instability frequency varies according to $f_0 = 0.02 U_j^{\frac{3}{2}}$ as expected (Laufer & Zhang 1983), and its non-dimensional value $f_0\theta_0/U_j$ is found to be a constant, close to the theoretical value of 0.017 (Michalke 1971). The amplitude of this instability wave increases exponentially as it is convected downstream; then it

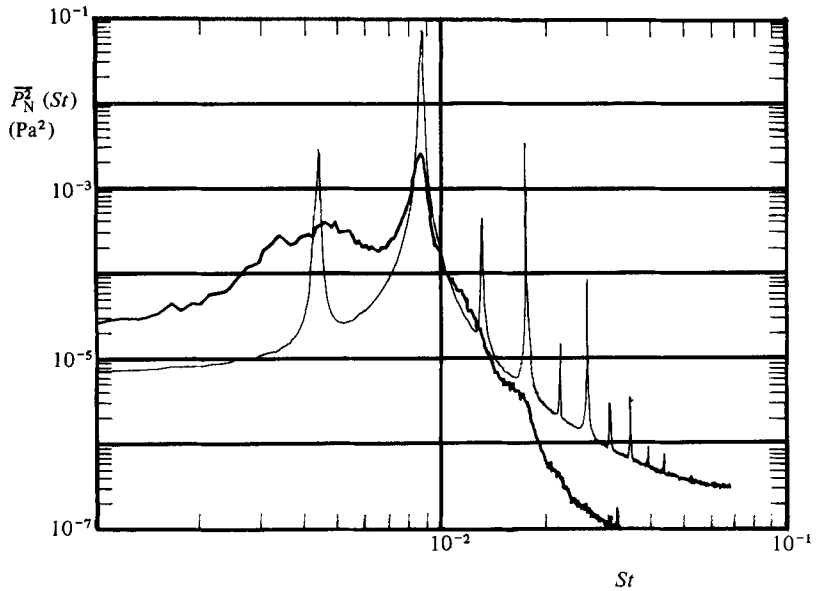

FIGURE 11. Near-field pressure specta, $U_j = 50$ m/s, $x/D = 0.20$: ——, natural; ——, excited.

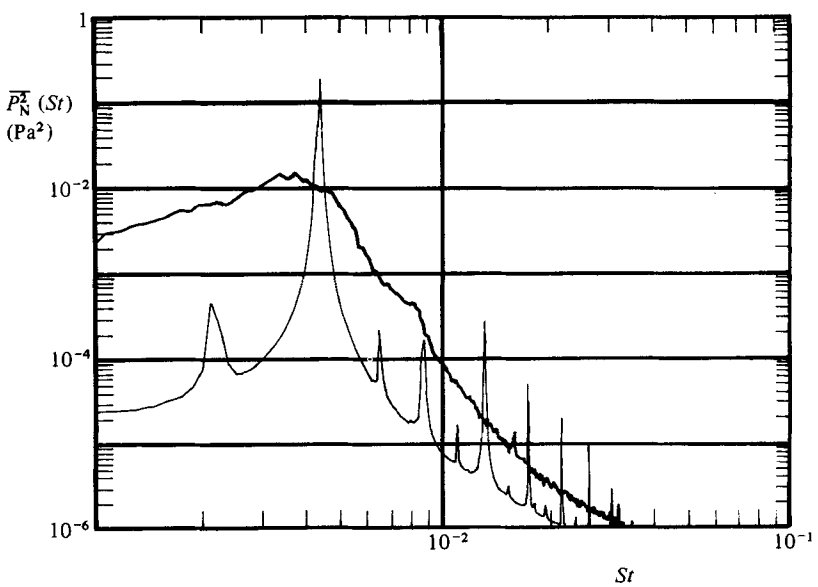

FIGURE 12. Near-field pressure spectra, $U_j = 50$ m/s; $x/D = 0.40$: ——, natural; ——, excited.

saturates and decreases. The first and second subharmonics behave in a similar fashion; in fact their saturation amplitude is even higher and occurs further downstream. A more detailed account of the mean and fluctuating velocity fields can be found in a recent paper by Laufer & Zhang (1983). They interpret the measurements in terms of vortex formation and vortex pairings in the shear layer: the saturation of the fundamental wave amplitude is associated with the periodic vortex formation,

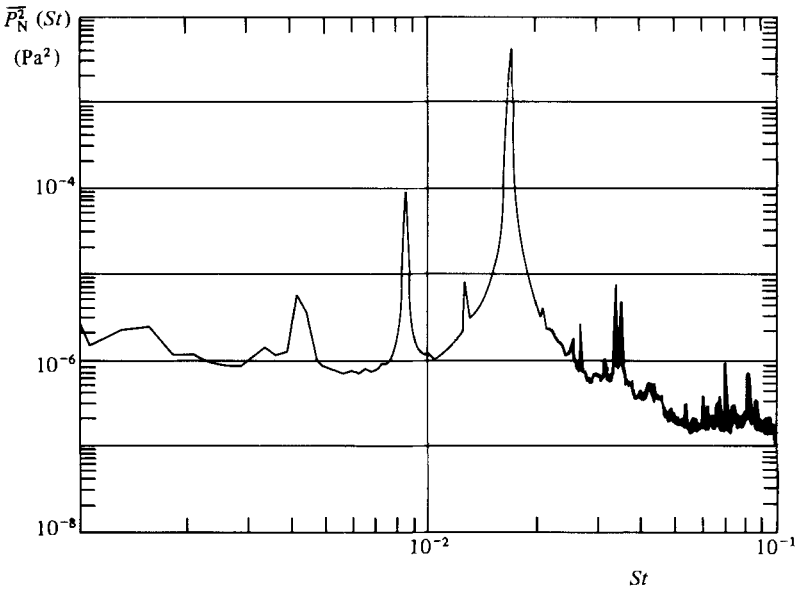

FIGURE 13. Near-field pressure spectra, $U_j = 30$ m/s; $x/D = 0.15$: ——, excited; $\overline{u_{m0}^2}/U_j^2 = 4 \times 10^{-3}$.

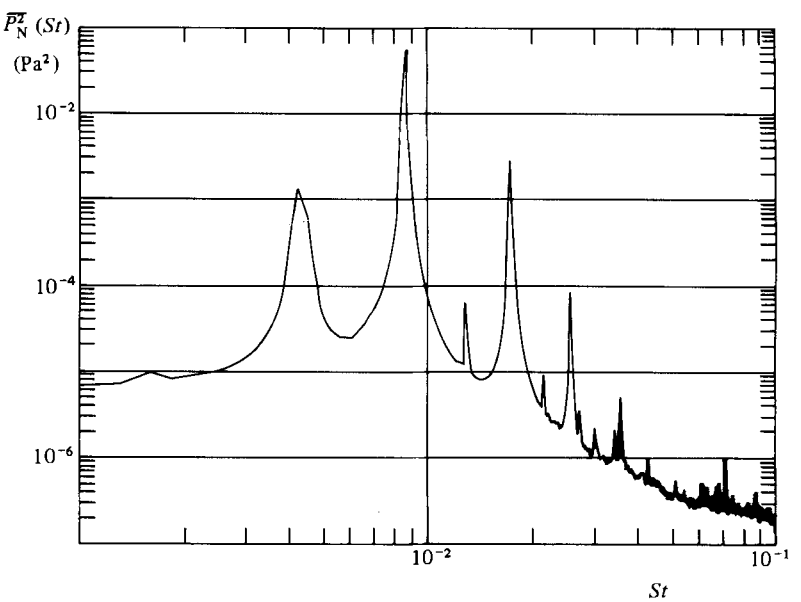

FIGURE 14. Near-field pressure spectra, $U_j = 30$ m/s; $x/D = 0.30$: ——, excited.

that of the first subharmonic amplitude with the first pairing and so on. This interpretation was first proposed by Ho & Huang (1982) for a two-dimensional mixing layer. Of particular interest is the almost stepwise increase of the momentum thickness associated with the pairing process.

Pressure spectra $\overline{p_N^2}(St)$ were obtained along a line making a 10° angle with the jet axis where $St \equiv f\theta_0/U_j$. Typical distributions are shown at three axial stations and

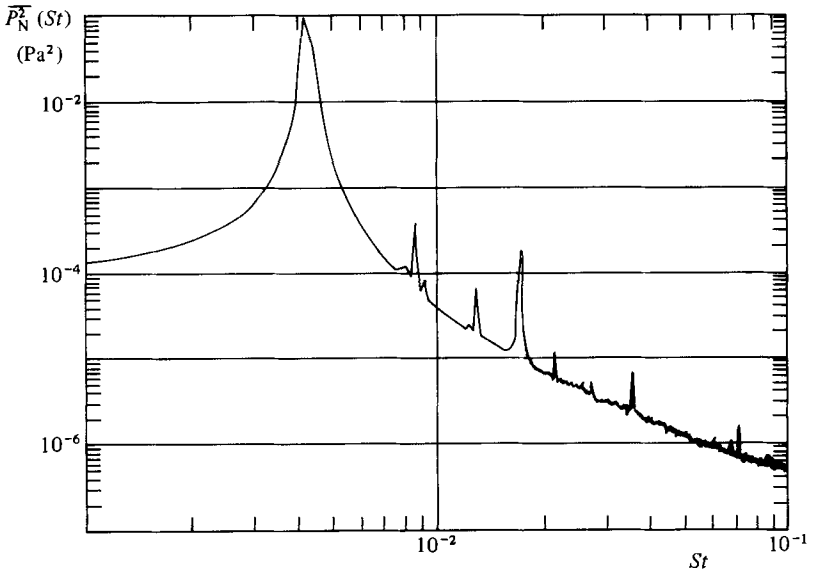

FIGURE 15. Near-field pressure spectra, $U_j = 30$ m/s, $x/D = 0.60$: ——, excited.

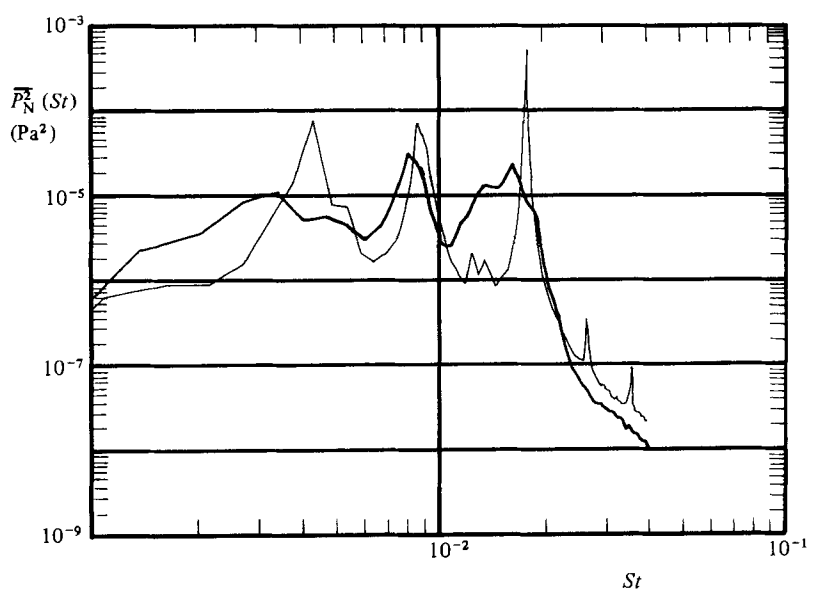

FIGURE 16. Near-field pressure spectra, $U_j = 18$ m/s, $x/D = 0.20$: ——, natural; ——, excited, $\overline{u_{m0}^2}/U_j^2 = 5 \times 10^{-4}$.

for four jet velocities in figures 7–18. The heavier lines correspond to the natural, that is, the unforced, case. The dominance of the fundamental is clearly seen at the first station; that of the first subharmonic at the second station close to where the first pairing takes place, while at the last station, near the second pairing location, the second subharmonic has most of the energy.

Since the interacting structures lose their coherence more and more after each successive coalescence and the phase fluctuation between interactions gets larger, it

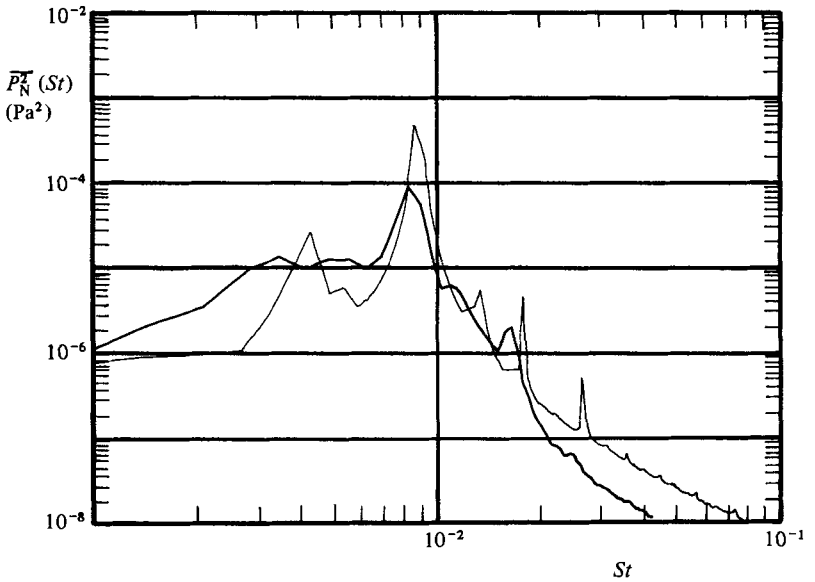

FIGURE 17. Near-field pressure spectra, $U_j = 18$ m/s, $x/D = 0.40$: ——, natural; ——, excited.

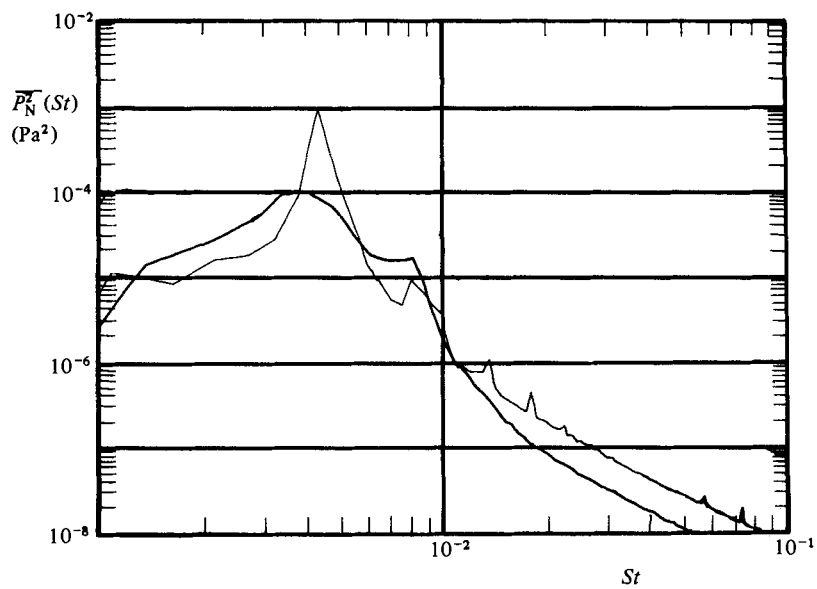

FIGURE 18. Near-field pressure spectra, $U_j = 18$ m/s, $x/D = 0.80$: ——, natural; ——, excited.

is to be expected that the measured spectrum peaks become weaker and broader for the lower subharmonics (see e.g. figure 9). As mentioned in §1, the spectrum broadening can be minimized by introducing at the nozzle exit an acoustic perturbation corresponding to the instability frequency of the initial shear layer, following Kibens (1980). Indeed, this technique did produce a more 'organized' jet; it localized the first three pairing positions, i.e. it minimized the random fluctuations of the positions where successive interactions occurred. As a result, the energy in the peaks increased

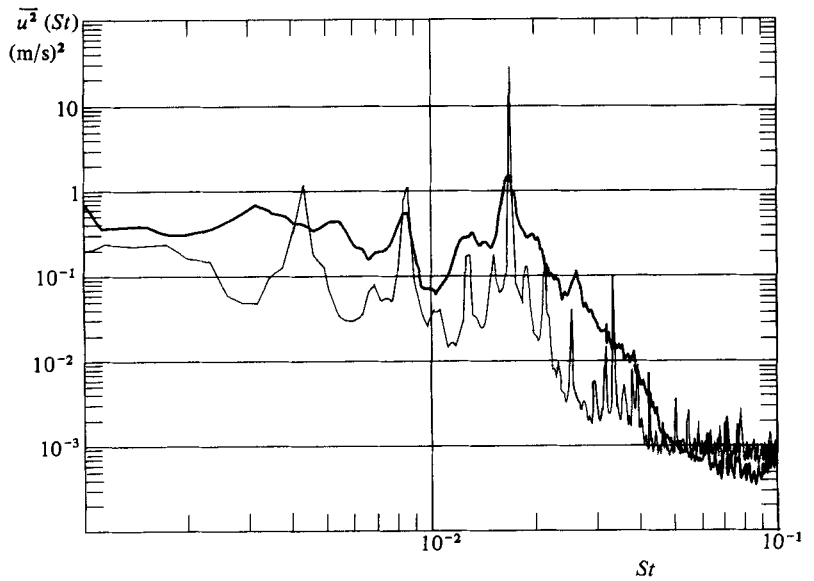

FIGURE 19. Velocity spectra, $U_j = 30$ m/s, $x/D = 0.15$, $y/D = 0.02$: ——, natural; ——, excited, $\overline{u_{m0}^2}/U_j^2 = 4 \times 10^{-3}$.

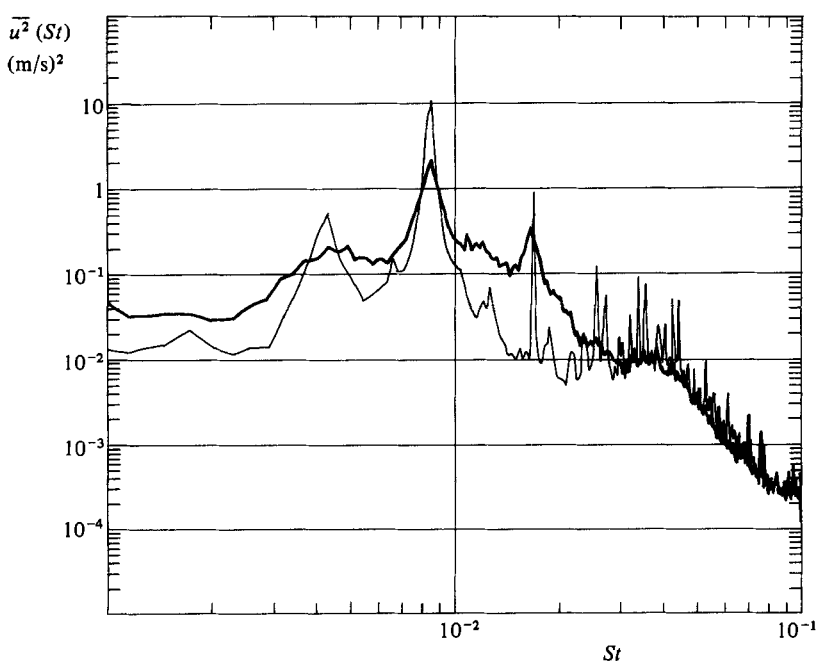

FIGURE 20. Velocity spectra, $U_j = 30$ m/s, $x/D = 0.30$, $y/D = 0.01$: ——, natural; ——, excited.

considerably, while that in the random, i.e. smooth, portion of the spectrum, especially at low frequencies, diminished. Comparison of the two curves shown in each of the spectra clearly shows this. It should be mentioned that this technique worked especially well in the mid-velocity range, in particular at 30 m/s. The accuracy

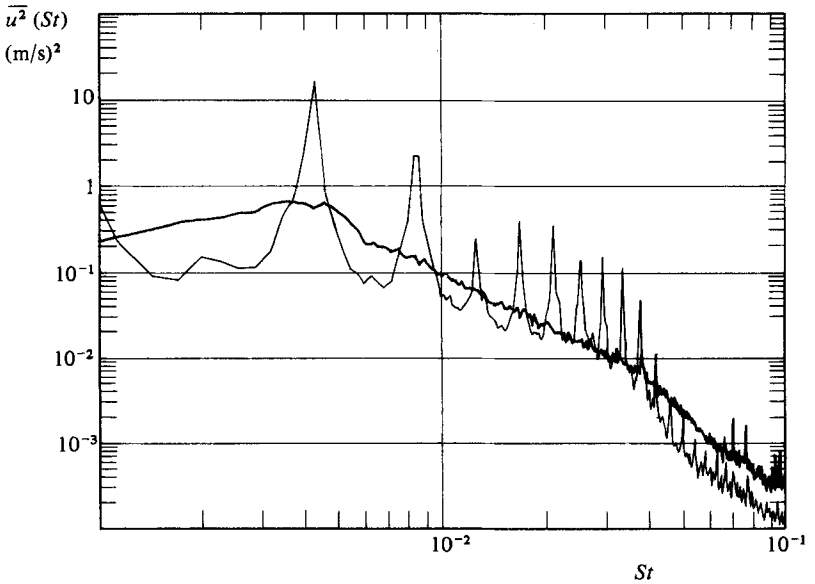

FIGURE 21. Velocity spectra, $U_j = 30$ m/s; $x/D = 0.60$, $y/D = 0.04$: ——, natural; ——, excited.

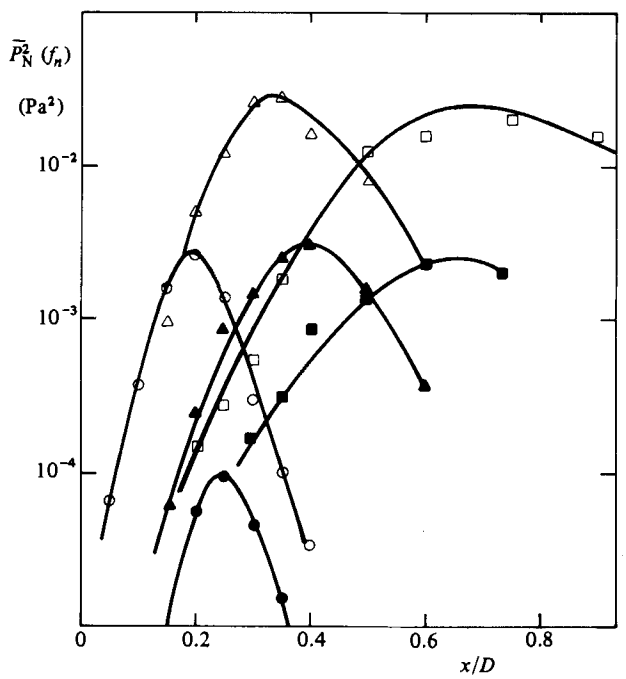

FIGURE 22. Axial variation of near-field pressure fluctuation. Open symbols: excited at $\overline{u_{m0}^2}/U_j^2 = 2.3 \times 10^{-3}$; solid symbols: natural. ●, ○, f_0; ▲, △, f_1; ■, □, f_2. $U_j = 30$ m/s.

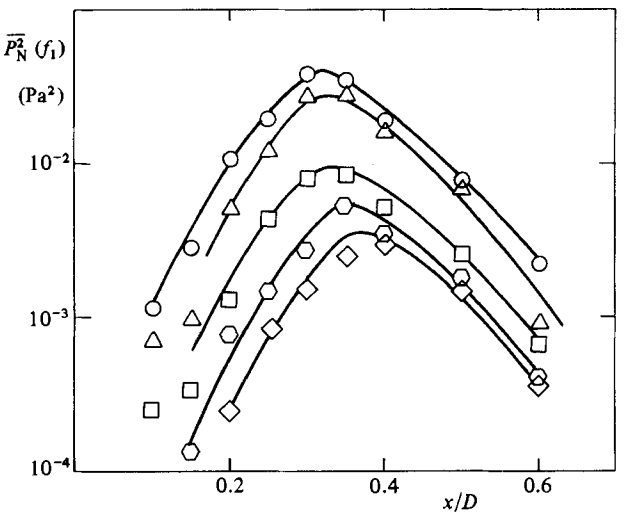

FIGURE 23. Axial variation of the first subharmonic pressure amplitude, $U_j = 30$ m/s: ○, $\overline{u_{m0}^2}/U_j^2 = 5.4 \times 10^{-3}$; △, 2.3×10^{-3}; □, 1.2×10^{-3}; ⬡, 6.2×10^{-4}; ◇, natural.

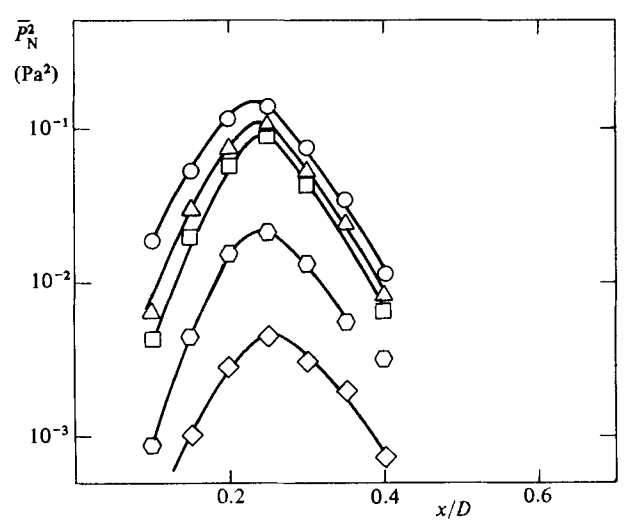

FIGURE 24. Axial variation of the first subharmonic pressure amplitude, $U_j = 50$ m/s: ○, $\overline{u_{m0}^2}/U_j^2 = 5.4 \times 10^{-3}$; △, 2.3×10^{-3}; □, 1.2×10^{-3}; ⬡, 6.2×10^{-4}; ◇, natural.

of the measurements was highest in this case, and therefore weighed more in drawing conclusions. At higher velocities it was found to be more difficult to lock into the natural instability frequency, consequently more scatter was encountered. At lower velocities the accuracy of the far-field measurements was hindered by the low level of radiation. It is also to be noted that apparently some amplitude modulation is taking place between interacting modes, since peaks at the sum and difference frequencies are evident.

For comparison a few velocity spectra are also shown for $U_j = 30$ m/s in figures 19–21. They were taken at radial positions corresponding to the maximum of a

U_j (m/s)	U_{cn}	M_{cn}	f_n (Hz)	λ_n	x_n (saturation location)	x_n (equation (1))	x_{sn} (equation (4))	U_{cn} (equation (5))
30	$0.52\ U_j$	0.046	1650	$0.19D$	$0.34D$	$0.34D$	$0.34D$	$0.51U_j$
30	$0.50U_j$	0.045	830	$0.36D$	$0.68D$	$0.69D$	$0.84D$	$0.51U_j$
50	$0.52U_j$	0.076	3600	$0.14D$	$0.24D$	$0.25D$	$0.25D$	$0.52U_j$
50	$0.50U_j$	0.074	1800	$0.28D$	$0.48D$	$0.50D$	$0.5D$	$0.50U_j$

TABLE 1

particular eigenmode. The effect of the excitation is quite similar to that found for the pressure fluctuations.

In order to see how the various instability-wave amplitudes evolve in the flow direction, figure 22 has been prepared, showing the mean-square amplitude distributions for the fundamental, first and second subharmonics, both with and without excitation. It is again to be noted that, even though the shear layer is artificially excited at its fundamental frequency, the subharmonics contain the larger maximum energy. Figures 23 and 24 show the distributions of the first subharmonic amplitudes at various excitation levels for two velocities, $U_j = 30$ m/s and 50 m/s. A number of features of these distributions should be pointed out: (i) the rapid increase and decrease in amplitude of each distribution; (ii) a similarity in their shape; (iii) the peaks occur at approximately the same axial location for a fixed Mach number. (There is a small but consistent shift that will be discussed subsequently.)

The third point is believed to be of special significance, since it is consistent with the conjecture of Laufer (1981) that the pairing locations (and the maximum fluctuations) are governed by a feedback mechanism according to the relation

$$\frac{x_n}{\lambda_n} = \frac{2}{1+M_{cn}}, \tag{1}$$

where x_n is the location of the nth pairing, λ_n is the wavelength of the nth subharmonic and M_{cn} the convection Mach number. For the present case table 1 gives a numerical comparison (here x_{sn} is the source location for the nth subharmonic, to be discussed later).

The distributions can be well approximated by a Gaussian

$$\overline{p_N^2}(f_n) = \overline{p_{Nm}^2}(f_n)\exp\left[-2\left(\frac{x-x_n}{\lambda_n}\right)^2\right], \tag{2}$$

where $\overline{p_{Nm}^2}$ is the saturation value of the mean-square pressure fluctuations (figure 25). It is to be noted that (2) is consistent with Crow's (1972) source model.

The convection velocities used above have been obtained by a standard technique; that is, by measuring the average phase difference in a narrow band frequency (corresponding to the fundamental and subharmonics) using two microphones at various axial distances apart. Typical measurements corresponding to two jet velocities are given in figures 26 and 27.

As mentioned earlier, the saturation location shifts slightly toward the nozzle as the excitation amplitude is increased. This is most probably a nonlinear effect. However, insufficient information is available to give a more specific explanation at this time.

Finally, it is of interest to examine the relationship between the velocity amplitude

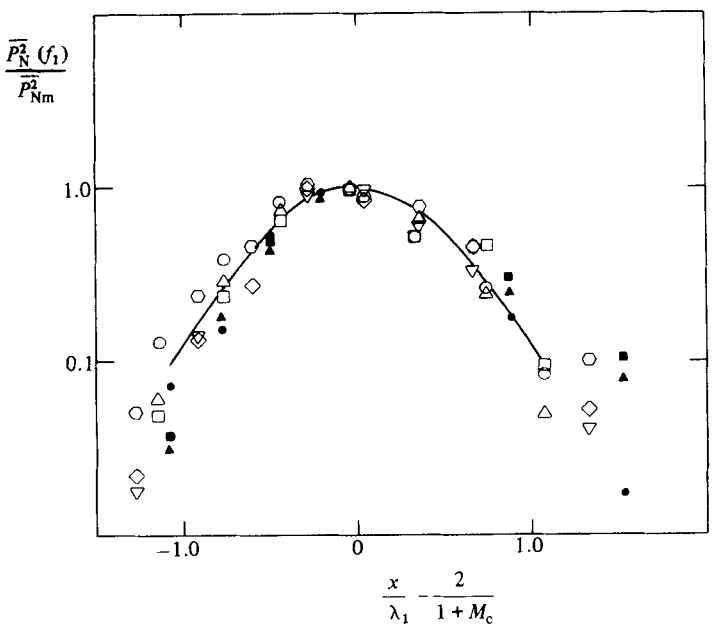

FIGURE 25. Variation of the normalized first subharmonic pressure amplitude.

$U_j = 50$ m/s	$U_j = 40$ m/s	$U_j = 30$ m/s
○ $\frac{\overline{u_{m0}^2}}{U_j^2} = 5.4\times10^{-3}$	○ $\frac{\overline{u_{m0}^2}}{U_j^2} = 5.4\times10^{-3}$	● $\frac{\overline{u_{m0}^2}}{U_j^2} = 5.4\times10^{-3}$
△ 2.3×10^{-2}	▽ 2.3×10^{-3}	▲ 2.3×10^{-3}
□ 1.2×10^{-3}	◇ 1.2×10^{-3}	■ 1.2×10^{-3}

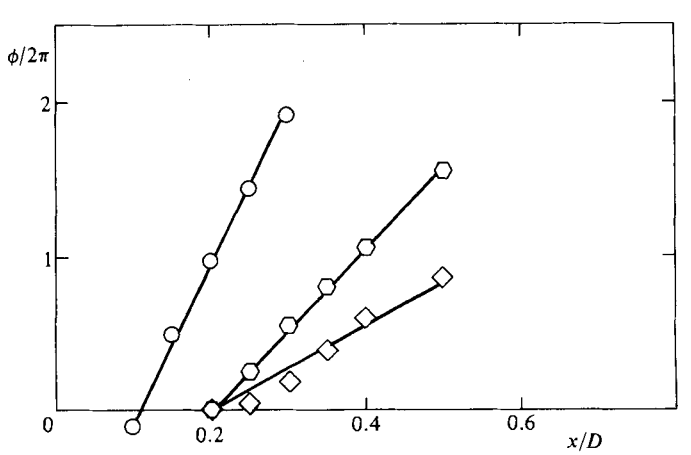

FIGURE 26. Axial phase-angle variation at $U_j = 30$ m/s: ○, f_0; ○, f_1; ◇, f_2.

$\overline{u_{mn}^2}$ and the induced maximum pressure field $\overline{p_{Nmn}^2}$ measured near the jet. Figure 28 shows this relationship for the three eigenmodes at a jet velocity of 30 m/s. It is seen that the dependence is linear. Subsequently, $\overline{u_{mn}^2}$ will be used as a reference when discussing the far-field radiation intensity.

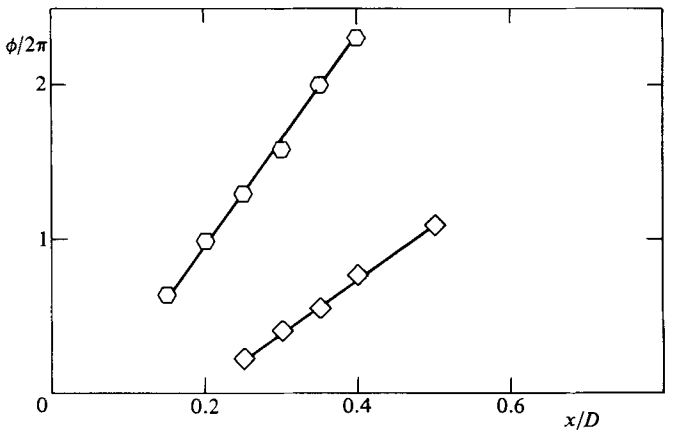

FIGURE 27. Axial phase-angle variation at $U_j = 50$ m/s: ○, f_1; ◇, f_2.

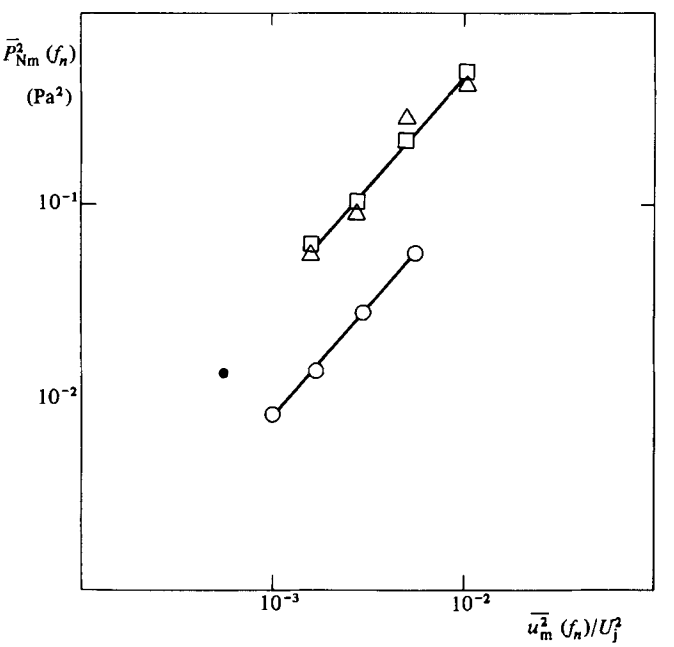

FIGURE 28. Relationship between the velocity eigenmode saturation amplitude and near-field maximum pressure amplitude, $U_j = 30$ m/s: ○, f_0; △, f_1; □, f_2.

3.2. *The far field*

At locations indicated in figure 3, pressure signatures were recorded and power spectra calculated by standard digital methods. The spectral distributions so obtained are presented in figures 29–32 for various forcing levels and jet velocities, and for $\theta = 30°$.

The strong peaks in the spectra are to be noted, in contrast with the usually smoother distributions measured at higher Mach numbers. Comparing the value of the peak frequencies to those obtained within and near the jet, no difference was detected. Interestingly, some of the weaker peaks corresponding to the sum and/or

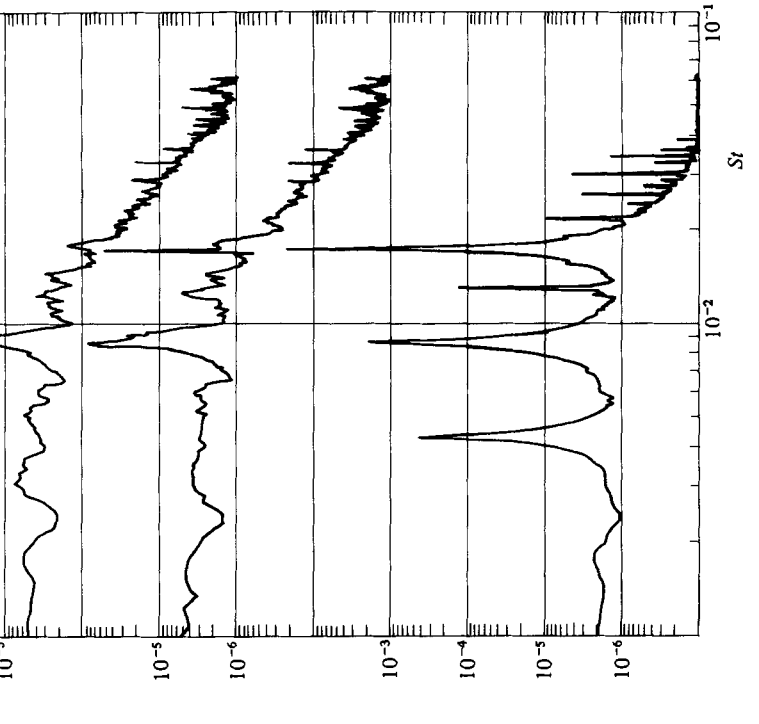

FIGURE 30. Far-field spectra, $U_j = 50$ m/s: top, natural; centre, $\overline{u^2_{m0}}/U_j^2 = 0.9 \times 10^{-3}$.; bottom, $\overline{u^2_{m0}}/U_j^2 = 1 \times 10^{-2}$.

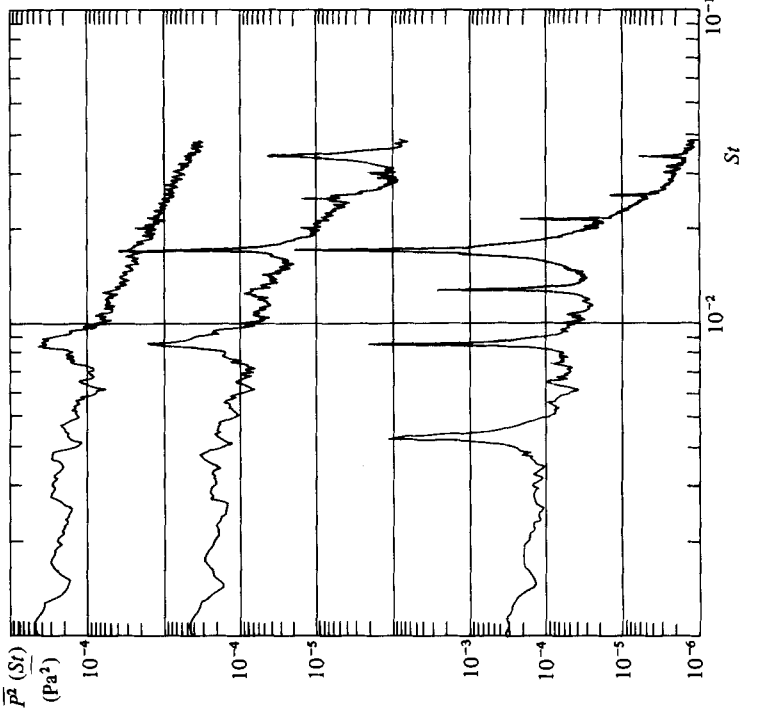

FIGURE 29. Far-field spectra, $U_j = 60$ m/s: top, natural; centre, $\overline{u^2_{m0}}/U_j^2 = 1.7 \times 10^{-3}$.; bottom, $\overline{u^2_{m0}}/U_j^2 = 1.3 \times 10^{-2}$.

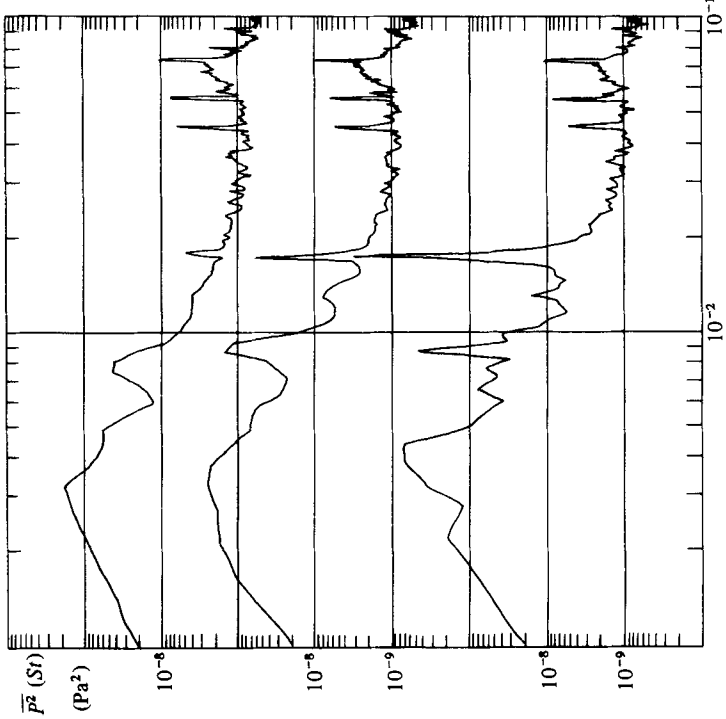

FIGURE 32. Far-field spectra, $U_j = 18$ m/s: top, natural; centre, $\overline{u_{m0}^2}/U_j^2 = 0.45 \times 10^{-4}$; bottom, $\overline{u_{m0}^2}/U_j^2 = 1.8 \times 10^{-3}$.

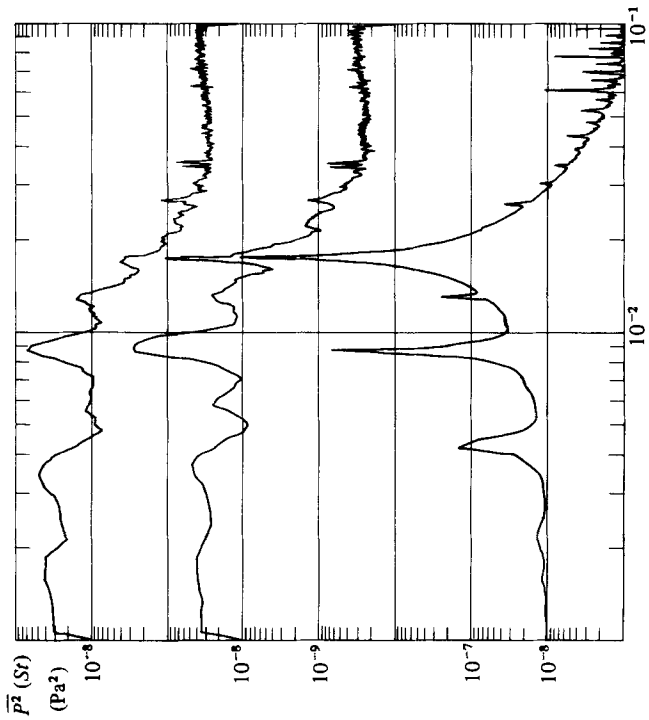

FIGURE 31. Far-field spectra, $U_j = 30$ m/s: top, natural; centre, $\overline{u_{m0}^2}/U_j^2 = 0.3 \times 10^{-4}$; bottom, $\overline{u_{m0}^2}/U_j^2 = 0.9 \times 10^{-2}$.

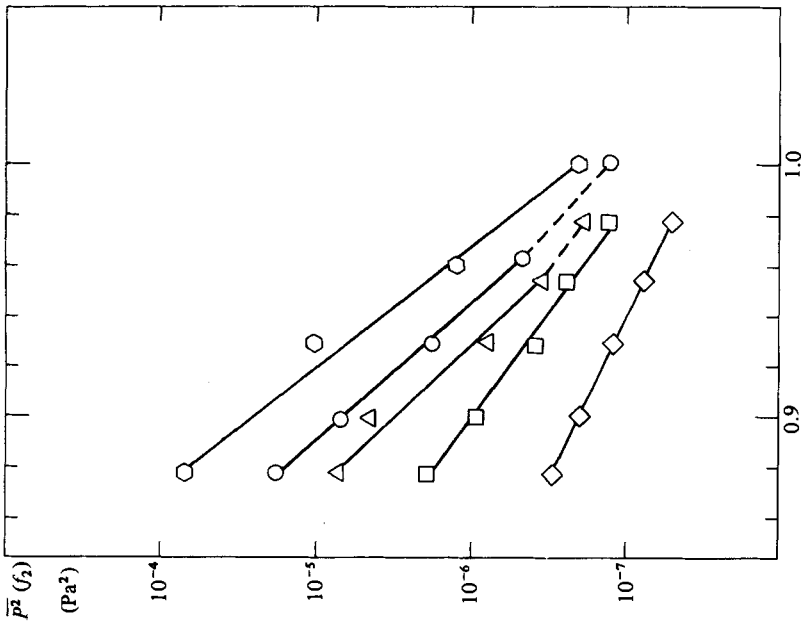

FIGURE 34. Directivity of the second subharmonic at various forcing levels, $U_j = 50$ m/s: ○, $\overline{u^2_{m0}}/U_j^2 = 5.8\times10^{-3}$; □, 1.5×10^{-3}; ○, 4×10^{-3}; △, 2.3×10^{-3}; ◇, natural.

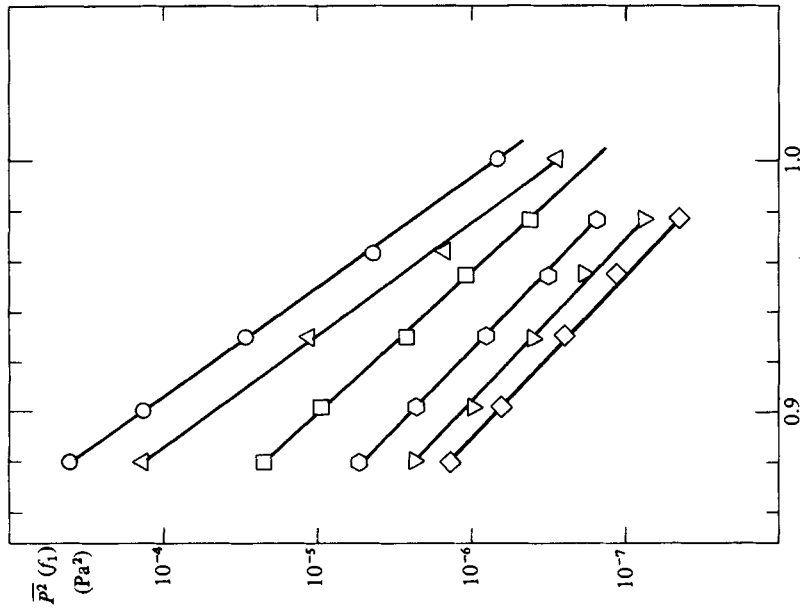

FIGURE 33. Directivity of the first subharmonic at various forcing levels, $U_j = 50$ m/s: ○, $\overline{u^2_{m0}}/U_j^2 = 4\times10^{-3}$; ○, 0.8×10^{-3}; △, 2.3×10^{-3}; ▽, 0.4×10^{-3}; □, 1.5×10^{-3}; ◇, natural.

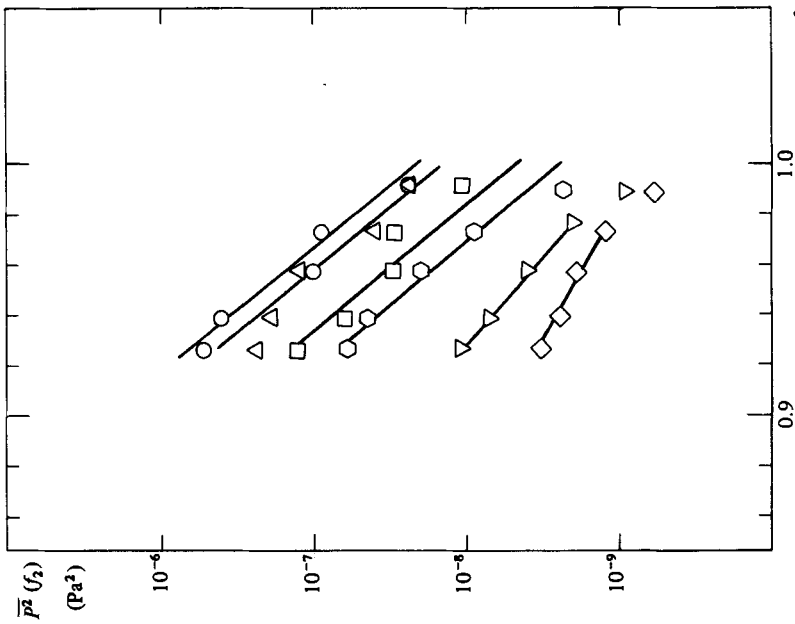

FIGURE 36. Directivity of the second subharmonic at various forcing levels, $U_j = 30$ m/s; ○, $\overline{u_{rms}^2}/U_j^2 = 4.0\times10^{-3}$; ⬡, 1.1×10^{-3}; △, 2.9×10^{-3}; ▽, 0.7×10^{-3}; □, 1.7×10^{-3}; ◇, natural.

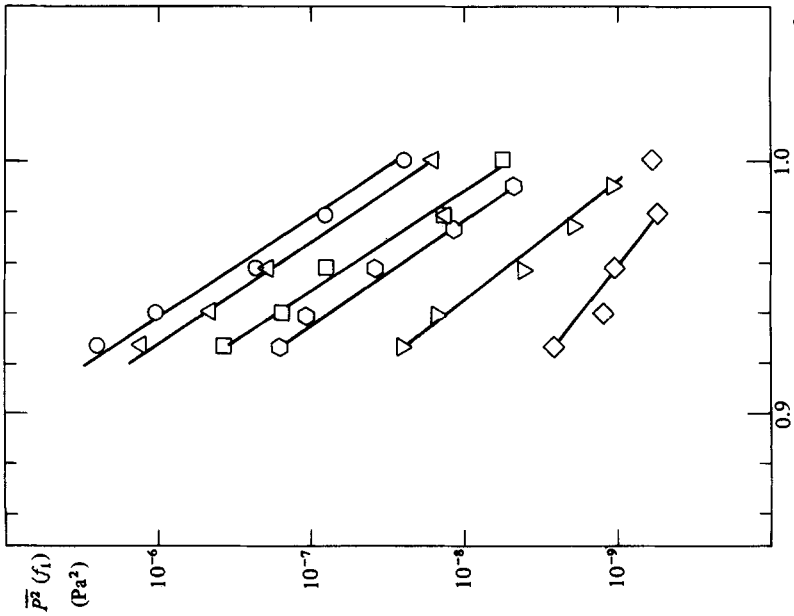

FIGURE 35. Directivity of the first subharmonic at various forcing levels, $U_j = 30$ m/s: ○, $\overline{u_{rms}^2}/U_j^2 = 4.0\times10^{-3}$; ⬡, 1.1×10^{-3}; △, 2.9×10^{-3}; ▽, 0.7×10^{-3}; □, 1.7×10^{-3}; ◇, natural.

difference of the eigenmode frequencies are also present in the far-field spectrum. Clearly, the measurements show no Doppler shift in frequency. It should be mentioned that, even though the jet velocities of the experiments are very low, any Doppler shift can be easily detected. (For instance, at 30 m/s and an angle of 30° the Doppler factor is 0.961, a shift well within the accuracy of the frequency measurement.)

The directionality characteristic of the radiation is shown in figures 33–36, where, for a fixed velocity and eigenfrequency, the variation of the far-field pressure fluctuations with the Doppler factor is shown for various excitation levels. A strong, exponential variation is to be noted. Interestingly, the slope of the curves is nearly a constant, close to -45, independent of the Mach number and excitation level, provided that the level is above a certain threshold value. It is conjectured that at lower levels (and with no excitation) phase fluctuations occur. That is, the saturation location of the unstable waves fluctuates in space, rendering the radiation less directional (cf. Ffowcs Williams & Kempton 1978).

4. Discussion

In the selected Mach- and Reynolds-number range, the measurements clearly indicate that, over the first diameter, the jet has a surprisingly well-organized flow field. Random fluctuations are caused primarily by phase fluctuations of the various instability waves, which in fact can be minimized by an appropriate excitation of the shear layer. Small-scale spatially random fluctuations contain negligible kinetic energy and play little role either in the flow development or in the radiation generation. This follows from the fact that the fluctuating field both in the near and far fields can be characterized by the length- and timescales of the instability waves only.

The time-dependent flow field can be thought of as the synthesis of a discrete number of interacting convected waves. The length of the initial wave is determined by the initial shear-layer thickness. After a rapid amplification–saturation–attenuation process, it is taken over by its first subharmonic, then by the second subharmonic and so on, each going through a similar growth–decay process. The mechanism – presumably nonlinear – that generates a subharmonic wave is not understood. It has been described in the literature in terms of vortex pairing (Winant & Browand 1974), a useful concept to visualize the process. Without a better understanding of this mechanism, any speculation concerning the nature and generation of an acoustic source in terms of the instability waves has to be done with some caution. It is clear that the Ffowcs Williams–Kempton 'vortex-pairing' model (which should more appropriately be called 'frequency-halving' model) is not realistic, since the predicted intensity is independent of the radiation direction, in contradiction with the present results. It is not clear *a priori* whether the measured radiation at a fixed frequency is generated by an instability wave of the same frequency or through the interaction of waves of different frequencies. This question has not been resolved in a definitive manner. However, it is believed to be significant that the strongest radiation from the undisturbed jet occurs at the subharmonic frequencies over the whole velocity range, and not at the fundamental. (This is probably the case for the excited jet as well; however, no conclusion can be drawn in that case since the spectrum peak at the fundamental frequency contains the energy radiated directly from the loudspeaker slot as well.) For this reason, special attention was focused on the subharmonics and, in particular, the first subharmonic radiation. In order to see what segment of the jet generates this frequency of radiation, pressure cross-spectrum measurements

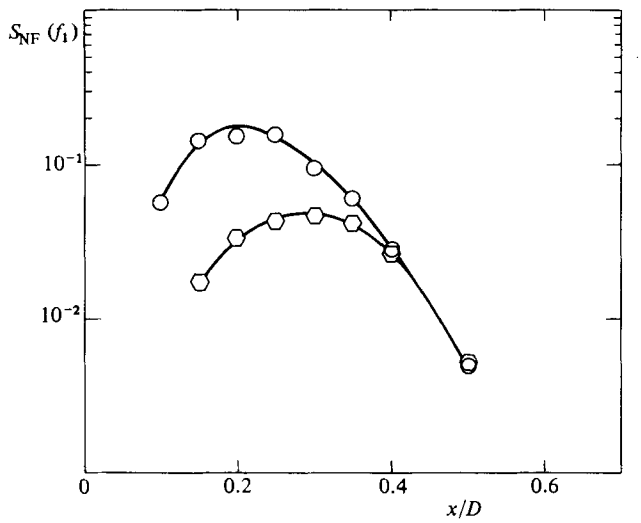

FIGURE 37. Near–far-field cross-spectra of the pressure fluctuations: ○, $U_j = 50$ m/s; ⬡, 30 m/s.

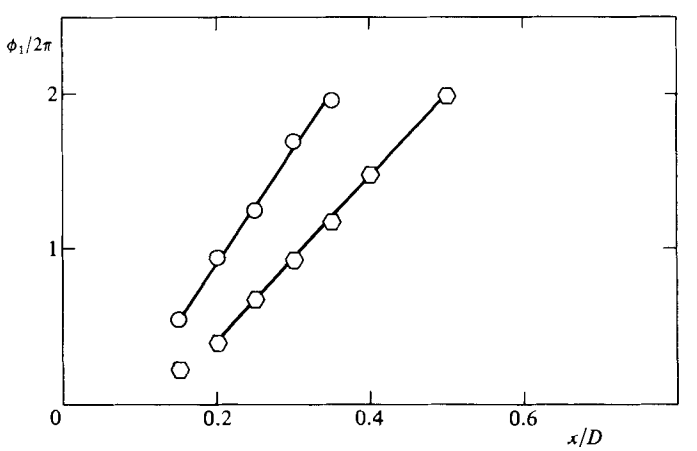

FIGURE 38. Phase-angle variation obtained from near–far-field cross-spectrum measurements at the first subharmonic: ○, 50 m/s.

were made between a fixed point in the far field ($\theta = 30°$, 2.55 m from the nozzle) and points along a 10° cone just outside of the jet (figure 3). The value of the normalized cross-spectrum at the first subharmonic frequency was then plotted against the near-field microphone position in figure 37 for two jet velocities. The distributions have a distinct maximum occurring at an axial location very close to that of the saturation point of the first subharmonic instability wave (table 1); that is, where the first pairing position is expected to occur. This result suggests that the subharmonic radiation is associated with the pairing process or – if one prefers to think in terms of convected instability waves – with the amplification–decay process of the subharmonic wave. In order to examine further this argument, phase-angle measurements between the near- and far-field microphones were also made (figure 38). Self-consistent results are obtained if the time delay between the signal of the

near-field microphone located at x and that of a far-field microphone located at a distance R from the acoustic source in the shear layer is expressed as

$$t_2 - t_1 = \frac{x - x_{sn}}{U_{cn}} + \frac{R}{a}. \tag{3}$$

This form was used by Hurdle & Meecham (1974) and by Peterson (1979 private communication). It is obtained under the assumption that the pressure signature detected at time t_1 by the near-field microphone is convected with velocity U_{cn} to the acoustic source location x_{sn} (i.e. the pairing location of the nth subharmonic) and then radiated with an acoustic velocity a to the far-field microphone located at a distance R from the source, and detected at time t_2. Equation (3) may be rewritten in terms of the phase angle as

$$\frac{\phi_n}{2\pi} = \frac{D}{\lambda_n}\frac{x - x_{sn}}{D} + \frac{R}{\lambda_{an}} - N, \tag{4}$$

where λ_{an} is the acoustic wavelength and the integer N is included to show the multivalued aspect of such a measurement. The results are shown in figure 38 for the first subharmonic at two jet velocities. From the slope of such distributions, one can obtain the convection velocity: dividing (4) by $2\pi f_n$ and differentiating, one obtains

$$2\pi f_n \frac{\mathrm{d}x}{\mathrm{d}\phi} = U_{cn}. \tag{5}$$

The phase angle that gives the source location ($x = x_{sn}$) is given by

$$\frac{\phi_{sn}}{2\pi} = \frac{R}{\lambda_{an}} - N. \tag{6}$$

The values of U_{cn} and x_{sn} are compared in table 1 with those obtained from near-field measurements. x_{sn} is seen to be close to the saturation location of the unstable waves, as well as to the calculated pairing positions.

In order to examine the variation of radiation intensity quantitatively, one may write the radiated mean-square pressure fluctuations of a fixed frequency in the following general form:

$$\overline{p^2(f_n)} = A^2_{\ell n} F\left(M_j, St_n, \frac{\theta_0}{D}\frac{D}{R}\right), \tag{7}$$

where $St_n \equiv f_n \theta_0 / U_j$. The convection Mach number is not shown explicitly, since it occurs as a constant percentage of the jet Mach number for the range of the present experiments. The factor expressed symbolically as $A^2_{\ell n}$ is a quantity related to the fluctuation amplitudes associated with the acoustic source. (It is written in this form to indicate that it might be related to two eigenmode parameters, n and ℓ.) Unfortunately, since the nature of the source is not known *a priori*, $A^2_{\ell n}$ cannot be written explicitly in terms of the flow parameters. However, the experimental results can be utilized to obtain some scaling laws. In particular, it is noted that, for a fixed M_j, varying the excitation level above a certain threshold value, the directivity characteristics of the radiation do not change, only its intensity. In this range of excitation, one finds that keeping F constant

$$\overline{p^2(f_n)} \sim (\rho_0 \overline{u^2_{mn}})^2 \tag{8}$$

within a reasonable accuracy. Figure 39 shows this variation for the first and second subharmonic radiation at $U_j = 30$ m/s. At other velocities more scatter was

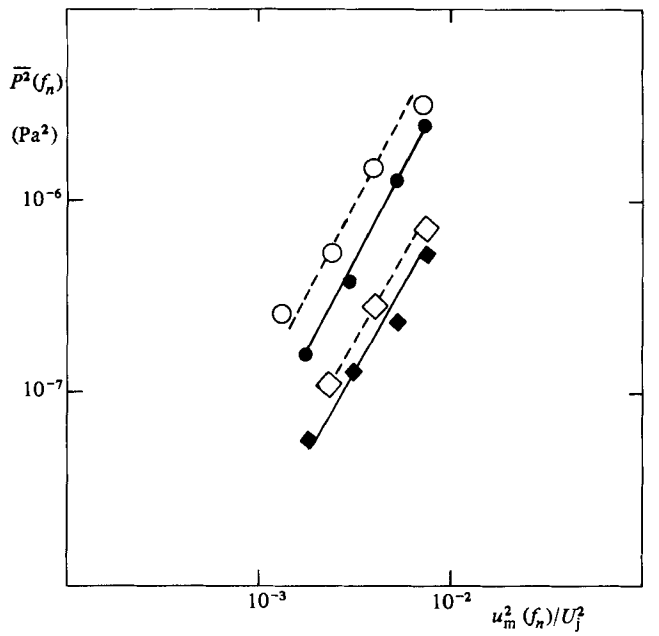

FIGURE 39. Variation of the far-field radiation intensity with the 30 m/s (○) saturation amplitude of the eigenmodes, $U_j = 30$ m/s, $\theta = 30°$. ●, f_1; ◆, f_2; ○, f_1; ◇, f_2 (repeat).

encountered. However, in all cases $\overline{p^2}$ varied faster than the first power of $\overline{u^2}$. This result is significant since it indicates some nonlinear behaviour associated with the acoustic sources.

Figure 39 also shows that the radiation intensity varies as the square of the frequency. Incorporating this result and the expected Mach-number variation, the experimental data were scaled according to the form

$$P \equiv \frac{\overline{p^2}(f_n)}{\rho_0^2(\overline{u_{mn}^2})^2} \frac{1}{M_j^4 St_n^2} \frac{R^2}{D^2} = F[(1 - M_c \cos\theta)^2] \tag{9}$$

and plotted as a function of the Doppler factor for various excitation levels at $U_j = 30$ m/s in figure 40. Figure 41 shows the effect of the Mach number. The solid line in figures 40 and 41 corresponds to the relation

$$P = 3 \times 10^2 \exp\{45[1 - (1 - M_c \cos\theta)^2]\}. \tag{10}$$

Considering the fact that P depends on the fourth power of the saturation amplitude of the instability wave, a quantity difficult to measure, and involves absolute intensities differing by a factor of 10^5, the self-consistency of the data can be considered satisfactory. Furthermore, since one is working with a highly 'tuned' system, the amplitude at the peak frequencies fluctuates considerably (especially at the lowest and highest velocities of the experiment), further impairing the accuracy of the measurements (see, for instance, the two sets of data shown in figure 39, taken approximately a year apart).

There are a number of comments one should make concerning the form of P in (9) and (10).

(i) The experimental character of the directivity is intimately connected with the

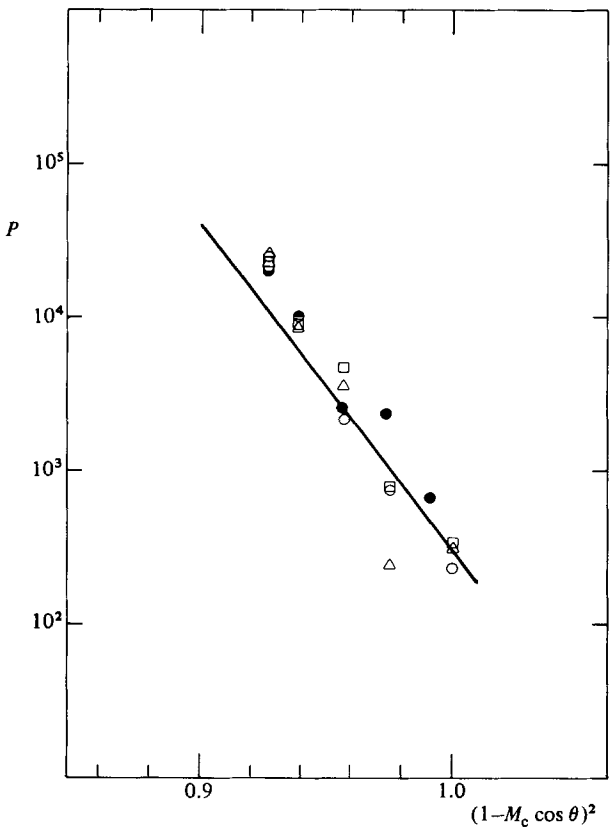

FIGURE 40. Normalized far-field radiation-intensity variation with the Doppler factor at various forcing levels and frequencies, $U_j = 30$ m/s. f_1: ○, $\overline{u_{m0}^2}/U_j^2 = 4.0 \times 10^{-3}$; △, 2.9×10^{-3}; □, 1.7×10^{-3}; ○, 1.1×10^{-3}. f_2: ●, $\overline{u_{m0}^2}/U_j^2 = 4.0 \times 10^{-3}$. The solid line corresponds to equation (10).

streamwise structure of the source. Clearly, the inclusion of the amplitude modulation of the instability wave is essential in properly describing the source. This is recognized in the 'wave-antenna' model but ignored in the 'frequency-halving' model.

(ii) The fact that the amplitude modulation occurs over several wavelengths suggests that the acoustic sources cannot be considered spatially compact in the flow direction. The presence of the Doppler factor in (10) is a consequence of this.

(iii) Within the accuracy of the measurements, the coefficient of the exponential function is a constant, independent of θ, a result inconsistent with a longitudinal and/or lateral quadrupole type of radiation.

(iv) As indicated earlier, the experiments shed no light on the apparently nonlinear generation of the source. It is puzzling to find that the near-field pressure fluctuations vary linearly with the velocity amplitudes of the instability waves (figure 28) while the far-field pressure fluctuations are best correlated with the square of the source-velocity amplitudes (figure 39). The model of Ffowcs Williams & Kempton (1978) is consistent with these results, but they give no justification or explanation for their choice of the nonlinear form.

(v) Finally, it should be emphasized that the results obtained here are applicable only in a limited Mach- and Reynolds-number range and apply to the radiation from the initial shear layer only. However, it is believed that the nature of the acoustic

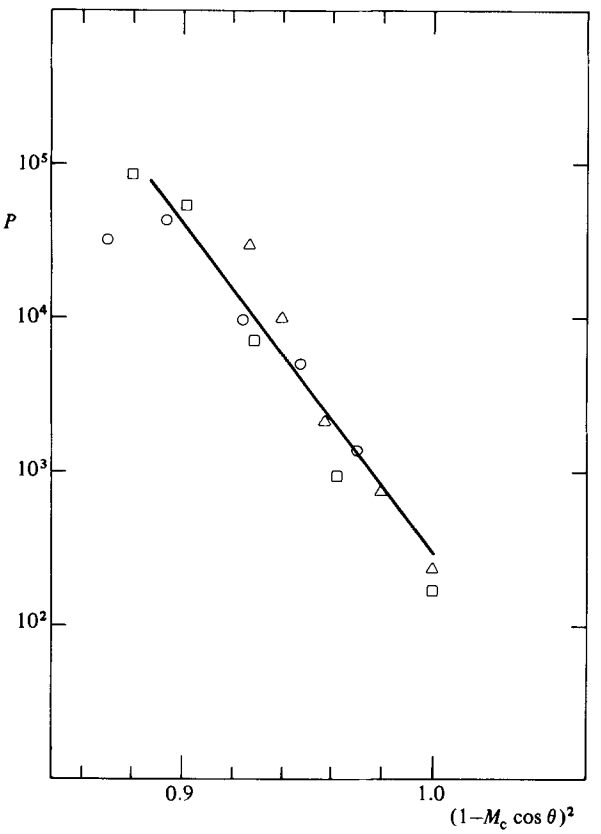

FIGURE 41. Normalized far-field radiation-intensity variation with the Doppler factor at various jet velocities ○, 70 m/s; □, 50 m/s; △, 30 m/s. The solid line corresponds to equation (10).

sources is basically the same for higher Reynolds and subsonic Mach numbers, except that in this range other modes and a wider spectrum of instability waves with more phase fluctuations are expected to take part in the radiation. Such a statement at this stage is, of course, only a conjecture, which has to be substantiated.

5. Conclusion

As pointed out in §1, the Lighthill formulation of the aeroacoustic problem serves well as a practical guide in focusing on the essential parameters governing the noise. However, it is not helpful in clarifying the physical mechanism of the noise generation. The main motivation of the present experiment was to shed some light on this mechanism, at least in a limited Mach- and Reynolds-number range.

The results show that the radiation within the first diameter of the jet is generated by convective instability waves developed on the shear layer. Their rapid axial amplitude variation – an amplification, saturation, attenuation sequence associated with the pairing process – produces a periodic thickening and thinning of the shear layer, which in turn generates a pressure field that develops into acoustic waves. Thus this rapid thickness variation over several wavelengths constitutes the acoustic source.

In the ideal situation, with no external flow perturbations present, the thickness

variation is fixed in space; the acoustic sources are thus stationary, radiating in discrete frequencies and no Doppler shift exists between source and radiation frequencies. (In the experiment this condition was simulated by exciting the initial shear layer at its most unstable frequency.) In the unforced case, the extraneous perturbations cause the thickness variation to move about axially, making the effective acoustic sources appear larger in extent, producing a spectrum broadening in the radiation field and decreasing the directivity of the radiation, while, in addition, they may introduce other instability frequencies. Incidentally, the decrease of the effective source size with excitation was also noted by Moore (1978) using a directional microphone.

Finally, it was found that the radiation is highly directional. This is closely related to the fact that the acoustic source has a (relatively large) spatial structure in the flow direction. The form of this structure has a strong influence on the directivity characteristics of the radiation.

The present results do not clarify the exact nature of the interaction between the instability waves or between the waves and the mean flow, but they do show that the resulting radiation intensity is proportional to the fourth, rather than the second, power of the maximum source amplitude fluctuations, suggesting a nonlinear source generation.

The authors are greatly indebted to Professor P. Monkewitz for his active interest and some helpful calculations that he made in order to clarify the implications of the line-antenna model. They also wish to acknowledge the helpful discussion they had with Professors C.-M. Ho, P. Huerre and D. Crighton.

This work was supported primarily by the NSF and with additional help from AFOSR.

REFERENCES

Bechert, D. & Pfizenmaier, E. 1975 On the amplification of broadband jet noise by pure tone excitation. *J. Sound Vib.* **43**, 581–587.

Browand, F. K. & Laufer, J. 1975 The role of large scale structures in the initial development of circular jets. In *Proc. 4th Biennial Symp. on Turbulence in Liquids, University of Missouri* (ed. J. L. Zakin & G. K. Patterson), pp. 333–344. Science Press.

Brown, G. L. & Roshko, A. 1974 On density effects and large structures in turbulent mixing layers. *J. Fluid Mech.* **64**, 775–816.

Crighton, D. G. 1975 Basic principles of aerodynamic noise generation. *Prog. Aerospace Sci.* **16**, 31–96.

Crow, S. C. 1972 Acoustic gain of a turbulent jet. *Bull. Am. Phys. Soc.*, paper IE.6.

Crow, S. C. & Champagne, F. H. 1971 Orderly structure in jet turbulence. *J. Fluid Mech.* **48**, 547–591.

Ffowcs Williams, J. E. & Kempton, A. J. 1978 The noise from the large scale structure of a jet. *J. Fluid Mech.* **84**, 673–694.

Ho, C. M. & Huang, L. S. 1982 Subharmonics and vortex merging in mixing layers. *J. Fluid Mech.* **119**, 443–473.

Hurdle, P. M. & Meecham, W. C. 1974 Investigation of the aerodynamic noise generating region of a jet engine by means of the simple source fluid dilatation model. *J. Acoust. Soc. Am.* **56**, 1708–1721.

Kibens, V. 1980 Discrete noise spectrum generated by an acoustically excited jet. *AIAA J.* **18**, 434–441.

Laufer, J. 1974 On the mechanism of noise generation by turbulence. *Omaggio a Carlo Ferrari*, pp. 451–464. Libreria Editrice Universitaria Levrotto & Bella, Torino.

LAUFER, J. 1981 Instability and turbulence in jets. In *Transition and Turbulence* (ed. R. E. Meyer), pp. 63–76. Academic.

LAUFER, J. & MONKEWITZ, P. 1980 On turbulent jet flows: a new perspective. *AIAA Paper* 80-0962.

LAUFER, J. & ZHANG, J-X. 1983 Unsteady aspects of a low Mach number jet. *Phys. Fluids* **26**, 1740–1750.

LIGHTHILL, M. J. 1952 On sound generated aerodynamically. I. General Theory. *Proc. R. Soc. Lond.* **A211**, 564–587.

MICHALKE, A. 1971 Instabilität eines kompressiblen runden Freistrahls unter Berücksichtigung des Einflusses der Strahlgrenzschichtdicke. *Z. Flugwiss.* **19**, 319–328.

MOORE, C. J. 1977 The role of shear-layer instability waves in jet exhaust noise. *J. Fluid Mech.* **80**, 321–367.

MOORE, C. J. 1978 The effect of shear layer instability on jet exhaust noise. In *Structure and Mechanisms of Turbulence II* (ed. H. Fiedler). Lecture Notes in Physics, vol. 76, pp. 254–264. Springer.

WINANT, C. D. & BROWAND, F. K. 1974 Vortex pairing: the mechanism of turbulent mixing-layer growth at moderate Reynolds number. *J. Fluid Mech.* **63**, 237–255.